Sensors and Actuators A 162 (2010) 336–347

Contents lists available at ScienceDirect

Sensors and Actuators A: Physical

journal homepage: www.elsevier.com/locate/sna

Characterization of piezoelectric PZT beam actuators for driving 2D scanning micromirrors

Kah How Koh[a], Takeshi Kobayashi[b], Fu-Li Hsiao[a,c], Chengkuo Lee[a,*]

[a] Department of Electrical & Computer Engineering, National University of Singapore, 4 Engineering Drive 3, Singapore 117576, Singapore
[b] National Institute of Advanced Industrial Science and Technology (AIST), 1-2-1 Namiki, Tsukuba, Ibaraki 305-8564, Japan
[c] Graduate Institute of Photonics, National Changhua University of Education, No. 1, Jin-De Road, Changhua City 500, Taiwan, ROC

ARTICLE INFO

Article history:
Received 30 September 2009
Received in revised form 2 April 2010
Accepted 12 April 2010
Available online 21 May 2010

Keywords:
Micro-electro-mechanical systems (MEMS)
Optical MEMS
Piezoelectric actuator
PZT
Micromirror

ABSTRACT

A silicon micromirror driven by piezoelectric $Pb(Zr,Ti)O_3$ beam actuators has been demonstrated for two-dimensional (2D) scanning mirror applications. Two devices of similar design with different dimensions have been fabricated. The Si mirror is micromachined from the device layer of an SOI wafer, while the piezoelectric beam actuator contains multilayers of $Pt/Ti/PZT/Pt/Ti/SiO_2/Si$ which is deposited and released from a SOI wafer. A 1×10 PZT arrayed actuator are separately arranged in parallel on a Si beam released from the SOI substrate after the micromachining process. The 10 PZT actuators are electrically connected in series. For the large micromirror device with mirror size of 5 mm × 5 mm, the first resonant frequency for bending mode was measured at 34 Hz, while the second mode, i.e., a twist mode or torsional mode, is measured at a resonant frequency of 198 Hz. For the small micromirror device with mirror size of 3 mm × 3 mm, the bending and torsional modes were observed at 122 Hz and 2.46 kHz respectively. 2D raster scanning patterns were illustrated for both micromirrors. dc superimposed bias effect was also investigated for both mirror sizes. With increased dc bias, larger deflection angles were obtained.

1. Introduction

Micro-electro-mechanical systems (MEMS) have demonstrated great promise in opening new frontiers in the applications such as energy harvesters, RF MEMS and optical MEMS. In the optical MEMS regime, micromirrors, microlens and gratings are driven to move or deform by actuators such that unique functions can be achieved in light manipulation such as, reflection, beam steering, filtering, focusing, collimating, and diffracting, etc [1,2].

In late 90s and early 2000, significant progress in the optical MEMS technology has been made in the telecommunication applications ranging from optical switches [3–4], variable optical attenuators (VOAs) [5–6] and tunable lasers [7–8]. On the other hand, Digital Light Processing (DLP) projectors based on the Digital Micromirror Device (DMD) developed by Texas Instruments in 1987 have been widely used nowadays [9]. More recently, development of handheld projectors based on using scanning mirror technology have become an intriguing killer applications in consumable electronics, IT and amusement business [10–13]. To display a much bigger image on an ordinary surface, e.g. a wall or a table, to show videos, movies and games is the missing link technology to be developed.

Scanning micromirror devices have been realized by using three actuation schemes: electromagnetic [14–18], electrostatic [19–23], electrothermal [24–28] and piezoelectric [29–33]. Electromagnetically actuated scanning mirrors can achieve large mechanical rotation angle but they require bulky external magnet cores for actuation, hence making compact packaging challenging. Electrostatic comb-drive mirrors have also been reported and despite being a versatile and simple actuation mechanism, there is low force generation, hence high biasing voltage is required. In addition, there is an electrostatic instability due to the pull in voltage and the optical behavior is largely non-linear, with the large cross-talk hindering an independent control of the angles. Electrothermal actuated micromirrors have simpler IC-compatible fabrication steps, with better optical performance as compared to the other actuation mechanisms. However, thermal actuators have inherent limitations for long term use due to silicon losing its nearly perfect linear elastic properties that make the material so attractive [34]. Another major disadvantage is their large power consumption and their optical behavior dependence on ambient temperature. On the contrary, piezoelectric actuated MEMS mirror scanners have low driving voltage, with highly repeatable and reliable results for MEMS applications. Piezoelectric material has the highest energy density as compared to other silicon based actuators [35–36], primarily due to their large dielectric strengths. For example, F. Filhol et al. have demonstrated a 1D resonant torsional micromirror based on PZT thin film actuation which can achieve an optical scanning

* Corresponding author. Tel.: +65 6516 5865; fax: +65 6779 1103.
E-mail address: elelc@nus.edu.sg (C. Lee).

0924-4247/$ – see front matter © 2010 Elsevier B.V. All rights reserved.
doi:10.1016/j.sna.2010.04.021

angle of 78° with less than 1 V_{pp} at 10.9 kHz in vacuum condition [30]. In another similar 1D PZT micromirror design proposed by J.-H. Park et al., a large optical scanning angle of 41° was obtained at resonance frequency of 28 kHz, 60 V_{pp} [33]. 2D optical micromirror based on PZT thick films has also been illustrated by Yasuda et al. in Japan [32]. Two orthogonal pairs of ring-actuators were used to compose a double-gimbal structure. When the actuators are biased independently, Lissajous scan patterns were realized.

Besides the difference in actuation mechanism, a wide variety of designs for 2D microscanners have also been reported in the literatures, with many of them deploying the two frame design for 2D actuation [17–18,31–32]. In the paper reported by a group of researchers from the University of Florida [25], bi-directional two-dimensional scanning was performed by fabricating two sets of large vertical displacement thermal microactuators on separate frames. The orthogonal orientation of the two sets of actuators results in two perpendicular axes of rotation for the micromirror. By biasing simultaneously both sets of actuators with ac voltage, Lissajous figures were obtained for their scanning mirror results. However, devices adopting the two frame actuation designs are often complicated and have to be realized by complex, time consuming fabrication processes, often accompanied by bulky packaging. Hence, it is important to create simpler single mirror design so that the device is able to achieve 2D scanning pattern under resonant condition.

For example, J.-C. Chiou et al. have reported a micromirror with large vertical rotation using electrostatic comb actuators fabricated at two opposite ends of the mirror [37]. Large static rotation, of various amplitudes, was also achieved through the application of a voltage that varies sinusoidal with time. This is due to the different harmonic modes experienced by the composite cantilever in the pre-stress comb-drive actuator (PCA).

A more straightforward and compact mirror design has been demonstrated by S. Schweizer et al. [38]. This design allows for orthogonal angular motions to be actuated by the same thermal bimorph, making 2D scanning possible through the simultaneous thermo-mechanical excitation of the "L"-shaped cantilever at non-resonance and resonance states. Mechanical scan amplitudes of over 15° in two orthogonal directions were obtained at a typical power of 5 mW. Another similar mirror design concept was developed by O. Isikman et al. in 2007 [39]. A magnetic permalloy film was electrodeposited on the mirror plate to aid vertical actuation while a composite polymer actuator connecting the mirror was used for out-of-plane actuation. Hence, 2D scanning can be achieved by using only one actuation coil. However, the presence of the external coil makes compact packaging highly demanding.

In this paper, we reported a novel scanning mirror driven by 1×10 PZT actuator array integrated on a silicon beam. A new 2D scanning actuation mechanism will be explored by adopting an analytical approach in the designing and modeling of the device. Finally, the actuator performance will be characterized for microscanner applications.

2. Design and modeling

A schematic diagram of the micromirror device demonstrated in this paper is shown in Fig. 1. Ten patterned PZT thin films are arranged in parallel along one of the sides of the micromirror. The PZT actuators are electrically connected in series, with the bottom

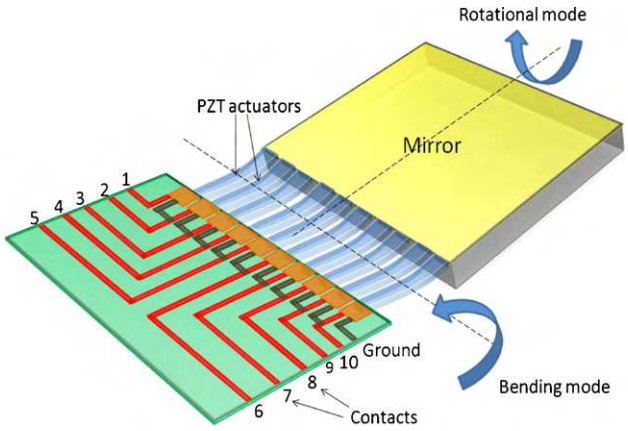

Fig. 1. Schematic drawing of MEMS scanning mirror where the mirror twists or bends due to ac voltage applied to the PZT actuators.

electrode of each actuator connected to the top electrode of the adjacent actuator. Two micromirror devices, with the same design but different dimensions, were investigated for 2D raster scanning. The dimensions of the 2 devices are summarized in Table 1.

The novelty of our scanner design lies in the mirror's ability to develop an out-of-plane degree of freedom and overcome the limitations of the actuation range of the PZT cantilevers. This is made possible from the knowledge that the microsystem of bending actuators and mirror being equivalent to a harmonic oscillator with a distributed mass suspended by a mechanical spring, hence making multiple resonant modes with all six degree of freedom of three-dimensional space to be probable. This phenomenon is supported by the finite element analysis (FEA) done using Abaqus v6.8 and shown in Fig. 2 where bending and torsional modes can be observed at different harmonic frequencies.

To evaluate the quality of the fabricated device, a model is necessary to compute the experimental displacement of the cantilever tip, so as to allow for comparison with the expected theoretical displacement. This allows for possible improvements to be made in the micromirror device's design and fabrication process, pushing the device to its projected performance.

The following equations are used to find the theoretical displacement of the actuator tip due to the contraction of the PZT film [40]:

$$\delta = \frac{3AB}{K} L^2 V d_{31} \tag{1}$$

$$A = S_{si}\ S_{PZT}(S_{PZT}\, t_{Si} + S_{Si}\, t_{PZT}) \tag{2}$$

$$B = \frac{t_{Si}(t_{Si} + t_{PZT})}{S_{PZT} t_{Si} + S_{Si} t_{PZT}} \tag{3}$$

$$K = (S_{si})^2 (t_{PZT})^4 + 4S_{si}S_{PZT}t_{Si}(t_{PZT})^3 + 6S_{si}S_{PZT}(t_{Si})^2(t_{PZT})^2 + 4S_{Si}S_{PZT}(t_{Si})^3(t_{PZT}) + (S_{PZT})^2(t_{Si})^4 \tag{4}$$

where δ is the displacement of the actuator, L is the length of the cantilever, V is the applied voltage, S_{si} and S_{PZT} are the compliances of the strutural Si layer (6.0×10^{-12} Pa^{-1}) and PZT thin film (1.43×10^{-11} Pa^{-1}) respectively, t_{Si} and t_{PZT} are the respective thicknesses of the strutural silicon and PZT film. The transverse piezoelectric constant, d_{31}, is assumed to be -50 p mV^{-1} when

Table 1
Dimensions of micromirror device A and B.

Device	Mirror	PZT actuators	Cantilever	Si mirror plate
A	5 mm × 5 mm	3 mm long × 0.24 mm wide × 3 μm thick	3 mm long × 5 mm wide × 5 μm thick	5 mm long × 5 mm wide × 0.4 mm thick
B	3 mm × 3 mm	0.5 mm long × 0.1 mm wide × 1 μm thick	0.5 mm long × 3 mm wide × 3 μm thick	3 mm long × 3 mm wide × 0.2 mm thick

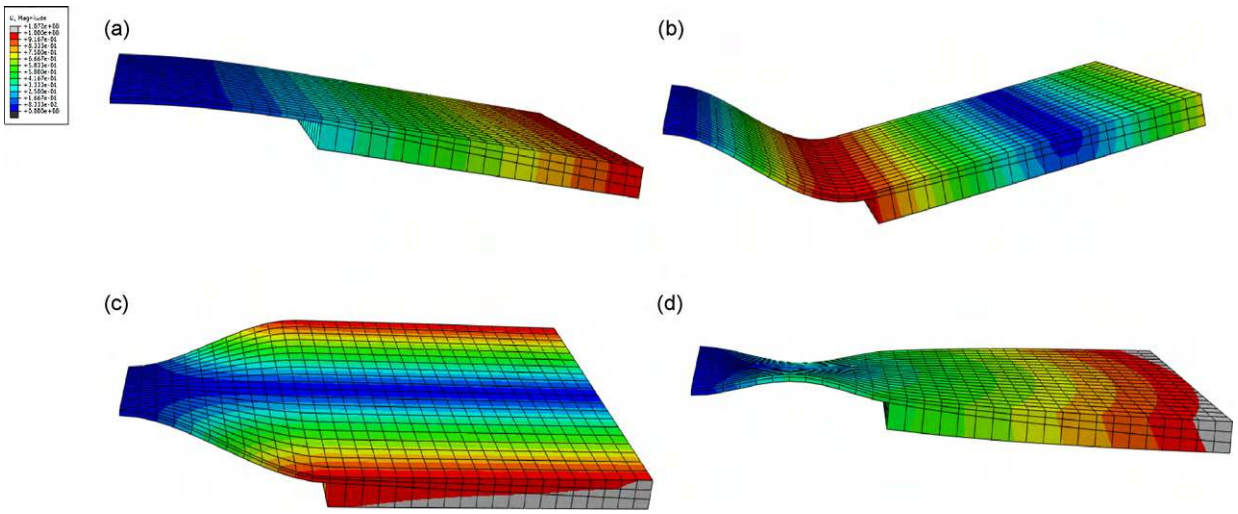

Fig. 2. Modal analysis of the scanning mirror using Abaqus (a) 1st bending mode: 6 Hz (b) 2nd bending mode: 33 Hz (c) 1st torsional mode: 121 Hz (d) 2nd torsional mode: 204 Hz.

calculating the theoretical actuated displacement caused by piezoelectric effect. The initial vertical displacement of the released PZT actuators was taken into consideration due to the expected dissimilarity in stress composition for the different deposited films. As a result, the total theoretical vertical displacement of an actuator is equivalent to the sum of initial displacement and actuated displacement when the actuator is electrically biased. This actuated displacement can be calculated using Eq. (1).

Fig. 3 is needed to calculate the total experimental displacement from the experimental data obtained. From Fig. 3, Eq. (5) can be derived:

$$\delta_T = r - r\mathrm{Cos}\theta_T \tag{5}$$

where δ_T is the total experimental vertical displacement of the cantilever tip, r is the radius of curvature, θ_T is the total mechanical deflection angle experienced by the cantilever under bias. Assuming θ_T is small, by small angle approximation,

$$\mathrm{Cos}\theta_T = 1 - \frac{1}{2}\theta_T^2 \tag{6}$$

$$r = \frac{L}{\theta_T} \tag{7}$$

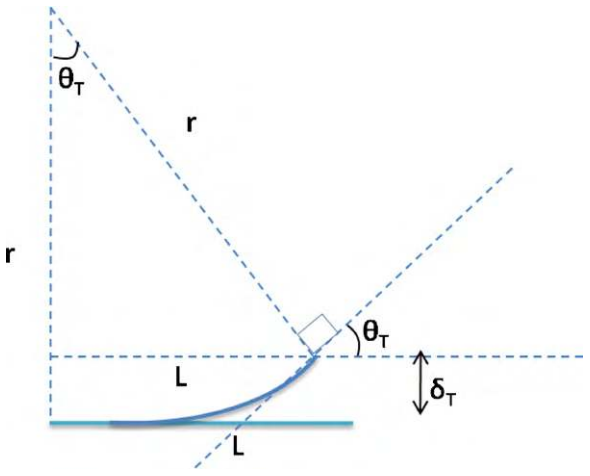

Fig. 3. Schematic drawing of biased PZT actuator with a total vertical displacement of δ_T and total mechanical rotation angle of θ_T.

Substituting Eqs. (6) and (7) into (5),

$$\delta_T = \frac{L(\theta_{PZT} + \theta_{initial})}{2} \tag{8}$$

where $\theta_{initial}$ is the initial mechanical rotation angle due to the release of stress in the actuator, θ_{PZT} is the mechanical rotation angle due to actuation by the cantilever under bias. $\theta_{initial}$ can be calculated from Eq. (9):

$$\theta_{initial} = \frac{2\delta_{initial}}{L} \tag{9}$$

where $\delta_{initial}$ is the initial vertical displacement of the released PZT cantilever. θ_{PZT} can be derived from the experimental data, to be presented later in the paper.

3. Device microfabrication

As shown in Fig. 4(a), a SOI substrate of 5 μm thick Si device layer and 1 μm thick buried oxide (BOX) was used as the starting material for micromirror device A. A thermal oxide layer of 0.37 μm was created from the Si device layer surface. Pt/Ti layers were deposited by sputtering to form the bottom electrodes, followed by deposition of 3 μm of PZT thin film by sol–gel process [41]. Finally, the top electrode is formed from multilayered deposition of Ti/Pt/Ti by sputtering. In Fig. 4(b), the top and bottom multilayered electrodes are etched away by Ar-ion while the PZT thin film were wet-etched away a mixture of HNO_3, HF and HCl [42]. In Fig. 4(c), a 0.8 μm thick oxide layer were deposited by RF-magnetron sputtering to serve as insulation. Contact hole etching were done by reactivce ion etching (RIE) with CHF_3 gas. In Fig. 4(d), Pt wire of 1 μm with Ti adhension was deposited by RF-magnetron sputtering and later etched by Ar ion. In Fig. 4(e), the thermal oxide, structural Si and BOX were etched by RIE using CHF_3 gas (SiO_2) and SF_6 gas (Si) to open the area of cantilever and mirror. Finally, in Fig. 3(f), the substrate Si and BOX were etched from the backside to release the mirror and the cantilever. A thick Si substrate is left beneath the mirror to maintain the rigidity and flatness of the mirror.

After the fabrication process, the device is bonded onto a metal package and the pads were connected by gold wire to the metal pins of the package as shown in Fig. 5. Gold sputtering was done on the mirror surface to improve its reflectivity. The initial vertical displacement of the released PZT cantilever of micromirror device A was measured by an optical microscope to be 300 μm. Fig. 6 shows the optical microscope photos of the various struc-

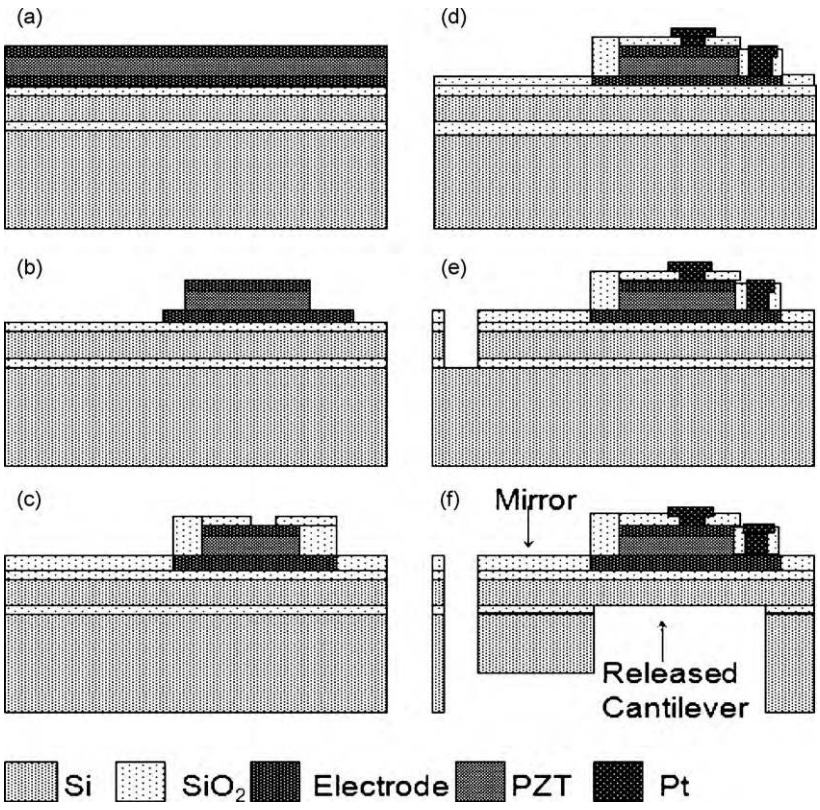

Fig. 4. Microfabrication process flow for making PZT actuators and mirror.

tures of micromirror device A. In Fig. 6(a) and (b), microphotos of the gold-coated mirror surface and the parallel arranged PZT actuators are illustrated respectively. Fig. 6(c) shows the serial electrical connection between adjacent actuators, where the top electrode of an actuator is connected to the bottom electrode of the adjacent electrode. Fig. 6(d) shows the individual contact pads connected to the bottom electrodes of their respective actuators. These contact pads are wire-bonded to a package as shown in Fig. 5 to allow for external biasing of device.

To elicit torsional and bending phenomenon in the device shown in Fig. 5, half of the actuators can be biased with an alternating voltage at one of the resonant frequency for bending mode while an alternating voltage at another resonant frequency for torsional mode was superimposed on the rest of the actuators. As such, the mirror will undergo both rotational and torsional bending simultaneously, forming two-dimensional high-speed raster scanning pattern.

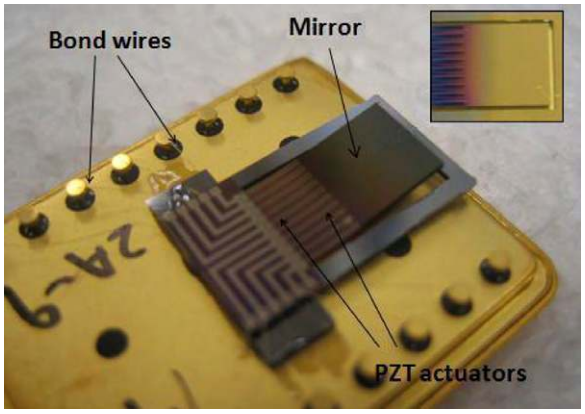

Fig. 5. A photo of the packaged MEMS micromirror device A with a mirror area of 5 mm × 5 mm. Inset picture shows a gold plated mirror surface of the device after gold sputtering.

4. Experimental setup

The schematic drawing of the measurement setup used in this experiment is illustrated in Fig. 7. A He/Ne laser source of wavelength 632.8 nm is used in this paper. The incident light from the source located at the left hand side is reflected by the mirror and propagates toward the screen on the right side with an optical deflection angle of 2θ, where θ denotes the mechanical deflection angle, which is the angle formed between the light paths of original state and biased state. The screen is placed and fixed perpendicularly to the reflected light when the mirror is initially unbiased. When the actuators are driven in ac mode, a mechanical deflection angle of $\pm\theta$ is introduced to the mirror. The resulted reflected light will be deviated from the original light path with an angle of $\pm 2\theta$ and the light spot on the screen will be shifted by a distance L. The value of θ can then be derived from the measured L and the known distance H, where H is the distance of the screen from the mirror. To enhance the piezoelectric characteristic of the actuators, poling treatment was done prior to the experiment at room temperature. A dc voltage of 25 V, which is equivalent to a polarization electric field of 83 kV/cm, was applied to each of the PZT plates for 5 min, with the poling direction from the bottom electrode to top electrode. Based on the approaches discussed previously in [43–44], we can estimate the transverse piezoelectric constant d_{31} of the PZT thin films. A 15% increase in d_{31} was noted before and after poling treatment.

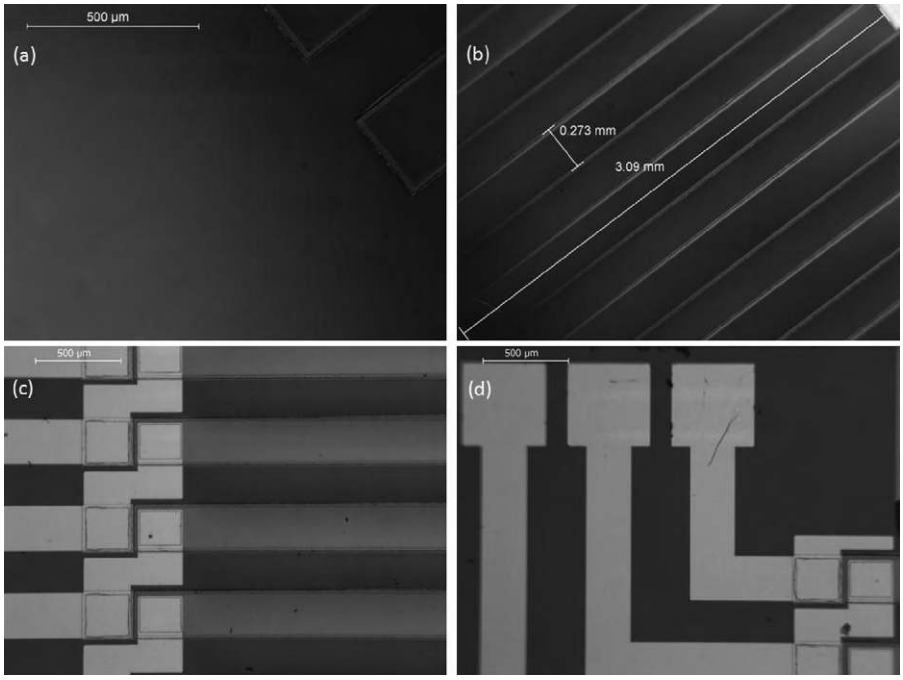

Fig. 6. Optical microscope photos of (a) gold-coated mirror surface (b) PZT actuators arranged in parallel (c) PZT actuators electrically connected in series, with the top electrode connected to the bottom electrode of the adjacent actuator (d) contact pads connected to the bottom electrodes of their actuators.

5. Results and discussion

5.1. dc characteristics

Fig. 8 shows the dc response for different biasing configuration made on micromirror device A while measuring the optical deflection angle. The mean dc driving voltage was obtained by taking the average of the voltage applied to each actuator when a bias is applied at one end of a set of serially connected actuators, while the other end is grounded. It can be seen clearly that optical deflection angle of micromirror device with PZT actuators 5–10 under bias was significantly higher than that of actuators 1–6 under the same bias. In other words, actuators 6–10 have better piezoelectric characteristics than actuators 1–5. This could possibly be resulted from a lithographic inaccuracy and deviation in fabrication steps for all the 1×10 PZT actuators, leading to the optical performance of the device as a whole being averaged out. When the 10th actuator was biased, the obtained optical deflection angle was poorer compared to the previous configurations. This is due to only one actuator being biased to actuate the mirror, whereas in each of the other two configurations, a total of six actuators were biased to help drive the mirror.

Fig. 9 shows the measured displacement of the PZT cantilever tip under bias and the theoretical displacement of the cantilever under non-resonant mode. The former was obtained by using the experimental data obtained previously for biasing configuration of actuators 5–10 and use them to calculate the mechanical rotation angle by Eqs. (8) and (9). To calculate the theoretical displacement

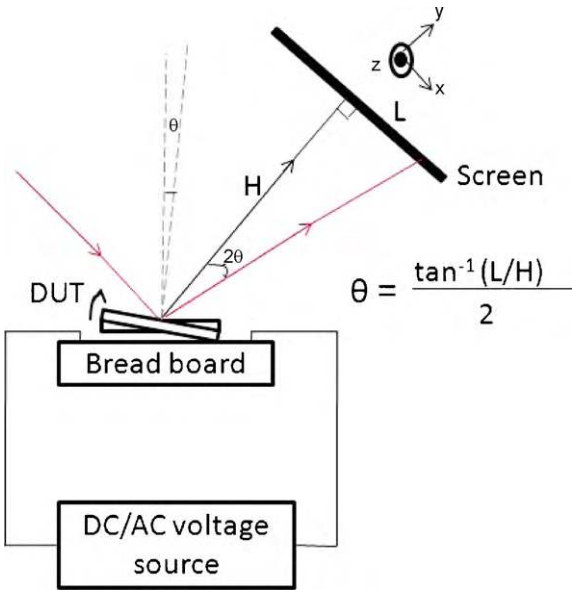

Fig. 7. Schematic drawing of measurement setup of mirror deflection angle when mirror is driven under dc or ac actuation voltage.

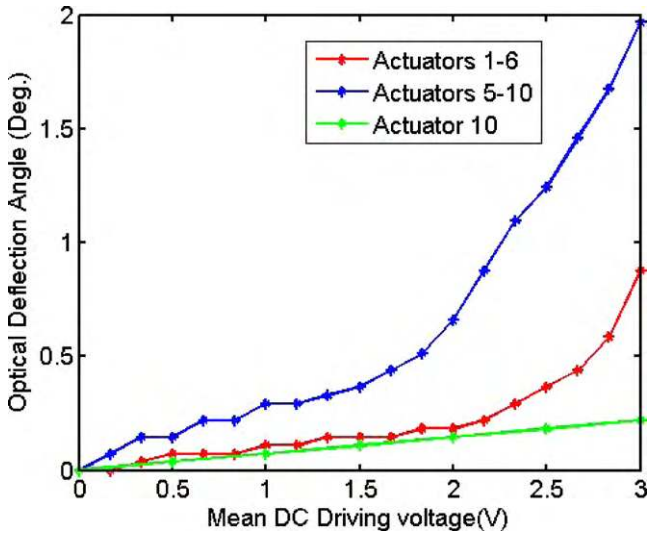

Fig. 8. Measured optical deflection angle versus mean dc driving voltage applied to each actuator for different biasing configuration of micromirror device A.

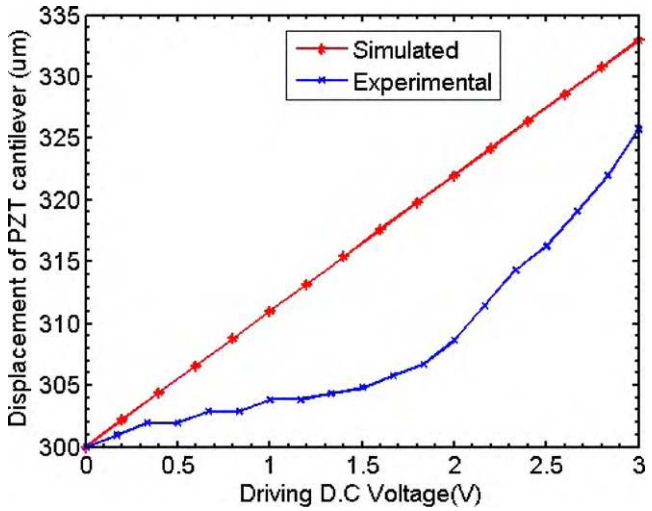

Fig. 9. Measured and calculated theoretical displacement of PZT cantilever tip for micromirror device A, based on experimental results and mathematical equations respectively.

of the actuator under dc bias, an initial vertical displacement of 300 μm was included in the calculation. The actuated displacement when the actuator is under bias can be calculated from Eqs. (1)–(4). The discrepancy between the theoretical and experimental data can be attributed to the mirror surface roughness, warpage of the mirror and fabrication inaccuracy. A non-linear experimental displacement-bias curve was obtained due to each actuator displaying varying piezoelectric characteristics.

5.2. ac characteristics

5.2.1. Micromirror device A

Fig. 10 shows the measured spectrum of optical deflection angle (2θ) with respect to ac voltage frequency varying from 0 Hz to 500 Hz, while 10 V_{pp} was applied to the actuators for different bias combinations. In Fig. 10(a), where only the 10th actuator was biased at 10 V_{pp}, two major peaks of 0.91° and 2.30° were observed at frequency of 17 Hz and 34 Hz respectively for bending mode. A minor peak of 0.37° was also detected at 460 Hz. For torsional mode, two optical deflection angle peaks of 0.59° and 0.67° were observed at resonant frequencies of 99 Hz and 198 Hz respectively. These resonant frequencies observed for both the bending and torsional mode coincides closely with the FEA simulation illustrated using Abaqus in Fig. 2. In Fig. 10(b), where 10 V_{pp} bias were applied across the serially connected actuators 1–6, i.e. a mean actuation bias of 1.67 V_{pp} applied to each actuator, peak deflection angles of 0.88° and 0.66° were observed at 17 Hz and 34 Hz respectively for the bending mode while peak angles of 0.74° and 0.56° were observed at 99 Hz and 198 Hz respectively for the torsional mode. However, in Fig. 10(c), where a mean actuation voltage of 1.67 V_{pp} were applied to each of the actuators 5–10, peak deflection angles of 1.10° and 3.0° were detected at 17 Hz and 34 Hz for bending mode, while a minor peak was detected for torsional mode of 0.45° was observed at 198 Hz. Hence, from the above results, it can be deduced that in order to achieve an optimum raster (torsional mode) and frame scan (bending mode) angles, the ideal bias configuration for micromirror device A will be to bias actuators 6–10 serially at 34 Hz for slow frame scanning and bias actuators 1–5 serially at 198 Hz for fast raster scanning.

In Fig. 11(a), the ac response of micromirror device A under resonant condition for bending mode was examined at 34 Hz. All the deflection-bias curves shown in Fig. 11(a) exhibited almost linear behavior. An approximate optical deflection angle of 2.8° were

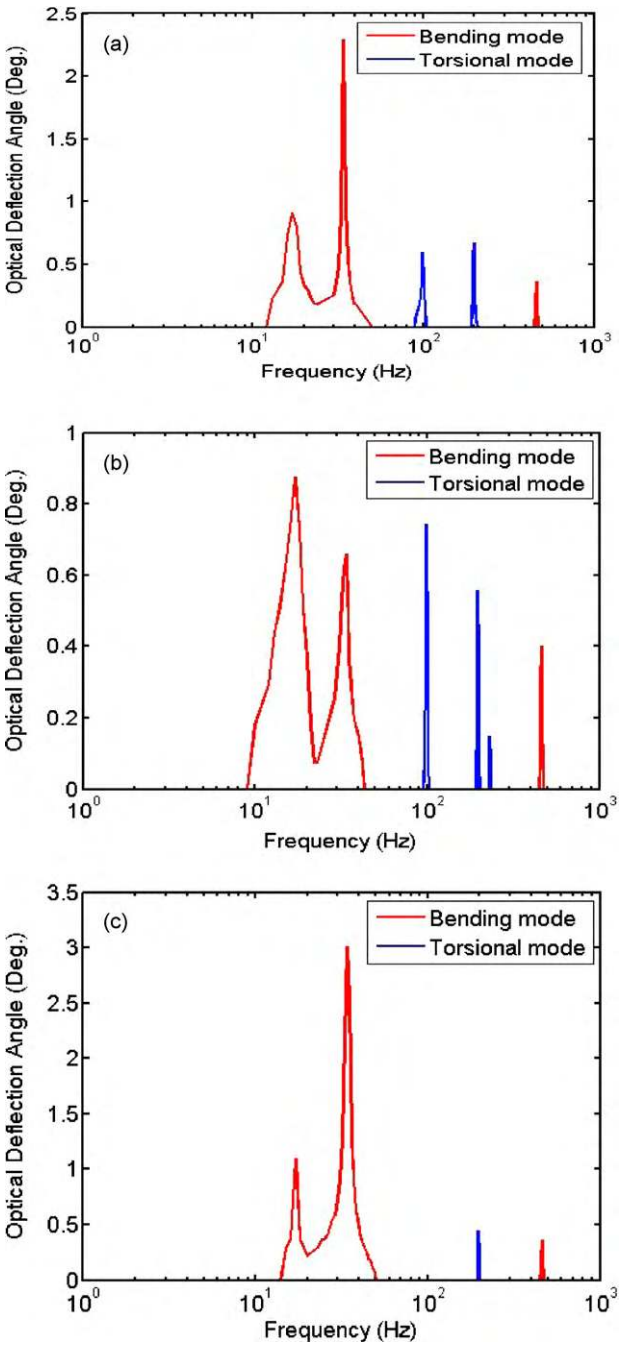

Fig. 10. Spectrum of optical deflection angle versus various ac actuation frequencies observed for both bending and rotation mode of the mirror micromirror device A, with (a) the 10th actuator biased at 10 V_{pp} (b) 10 V_{pp} biased serially to actuators 1–6, actuators 7–10 unbiased (c) 10 V_{pp} biased serially to actuators 5–10, actuators 1–4 unbiased..

obtained when the serially connected actuators 5–10 were biased at 9 V_{pp} i.e. a mean voltage of 1.5 V was applied to each actuator. In the case when actuators 1–6 were each biased at 1.5 V_{pp}, an optical deflection angle of only 0.6° was obtained. This is due to the observation discussed earlier in dc characteristics, where the piezoelectric characteristic of actuators 1–6 is weaker compared to actuators 5–10. When the 10th actuator was biased under resonant condition, the optical deflection angle was considerably smaller when compared to the other biasing configurations. This inferior performance is expected as only 1 actuator is involved in the actuation process. Fig. 11(b) shows the measured optical deflection angle

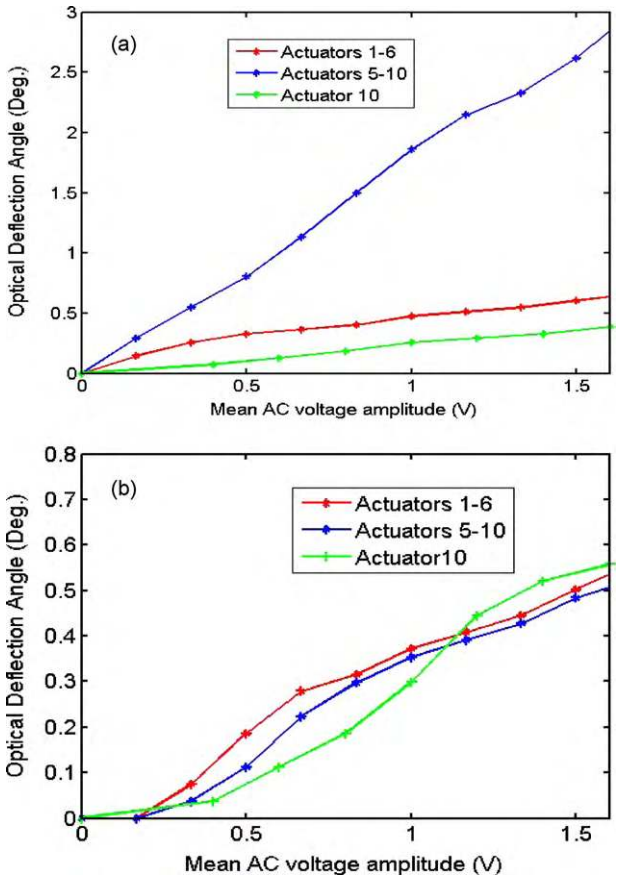

Fig. 11. Measured optical deflection angle of micromirror device A versus mean ac driving voltage for different biasing configuration, at (a) secondary bending mode frequency of 34 Hz (b) torsional mode frequency of 198 Hz.

obtained in torsional mode at resonant frequency of 198 Hz when different biasing configuration were applied to micromirror device A. Negligible difference in optical deflection angles were observed when biasing actuators 1–6 and actuators 5–10 under torsional mode.

In Fig. 12, the effect of dc bias on optical deflection angle was investigated on a single actuator, where a dc bias was superimposed on an alternating voltage. For the same ac voltage amplitude applied to the 10th actuator in bending mode, a greater dc offset resulted in a bigger optical deflection angle. The optical deflection angle can reach as high as 5° with 2 V dc offset and 6 V_{pp} superimposing at a resonant frequency of 34 Hz, However, a deflection angle of only 1.46° was obtained for the zero dc offset case at 6 V_{pp}. This is because when dc bias was applied to the PZT thin film in the actuator, the piezoelectric constant i.e. d_{31} increased due to *in situ* poling effect. This trend coincides with the result drawn in our previous study earlier in ref. [45].

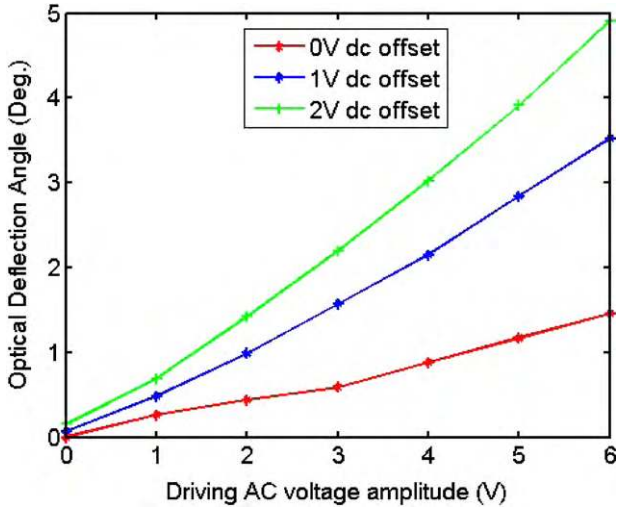

Fig. 12. Measured optical deflection angle of micromirror device A versus ac driving voltage obtained when the 10th actuator is biased simultaneously with an ac voltage at a frequency of 34 Hz and various dc offset.

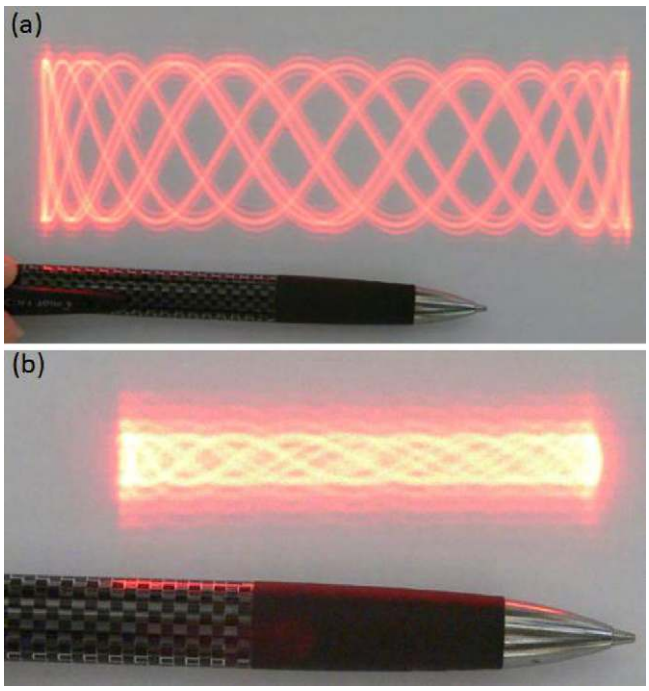

Fig. 13. (a) Lissajous scan pattern obtained when actuators 5–10 are serially biased at 34 Hz, 6 V_{pp}, and actuators 1–4 are serially biased at 198 Hz, 10 V_{pp}. (b) Lissajous scan pattern obtained when actuators 1–4 are serially biased at 34 Hz, 10 V_{pp}, while actuators 5–10 are serially biased at 198 Hz, 10 V_{pp}.

Fig. 13 illustrates the laser scanning pattern for micromirror device A. For the device to obtain 2D scanning capability, the slow and fast scan drive signals are superimposed, with half of the actuators biased at 34 Hz, bending mode while the other half of the actuators biased at 198 Hz, torsional mode. This resulted in Lissajous scan patterns obtained in Fig. 13a and b.

5.2.2. *Micromirror device B*

A new micromirror device B of the same design but of smaller dimensions as listed in Table 1 was investigated for ac characterization. In Fig. 14(a), where only the 10th actuator was biased at 10 V_{pp}, resonant peaks for bending mode were observed at 61 Hz and 122 Hz with optical deflection angles of approximately 0.97° and 2.80° respectively. For torsional mode, maximum optical deflection angle of approximately 0.20° and 0.40° were noted at 1.23 kHz and 2.46 kHz. As shown in Fig. 14(b), when serially connected actuators 1–6 were biased at 10 V_{pp}, i.e. a mean actuation bias of 1.67 V_{pp} applied to each actuator, peaks of 0.12° and 0.15° were observed at 61 Hz and 122 Hz respectively. A peak of 0.14° was observed at 2.46 kHz for torsional mode. In Fig. 14(c), a mean actuation voltage of 1.67 V_{pp} was applied to each of the actuators 5–10. It can be seen that actuators 5–10 responds better to bending mode, with peaks of 1° and 1.2° at 61 Hz and 122 Hz respectively. During torsional mode, peaks of 0.17° and 0.2° were recorded at 1.23 kHz and 2.46 kHz.

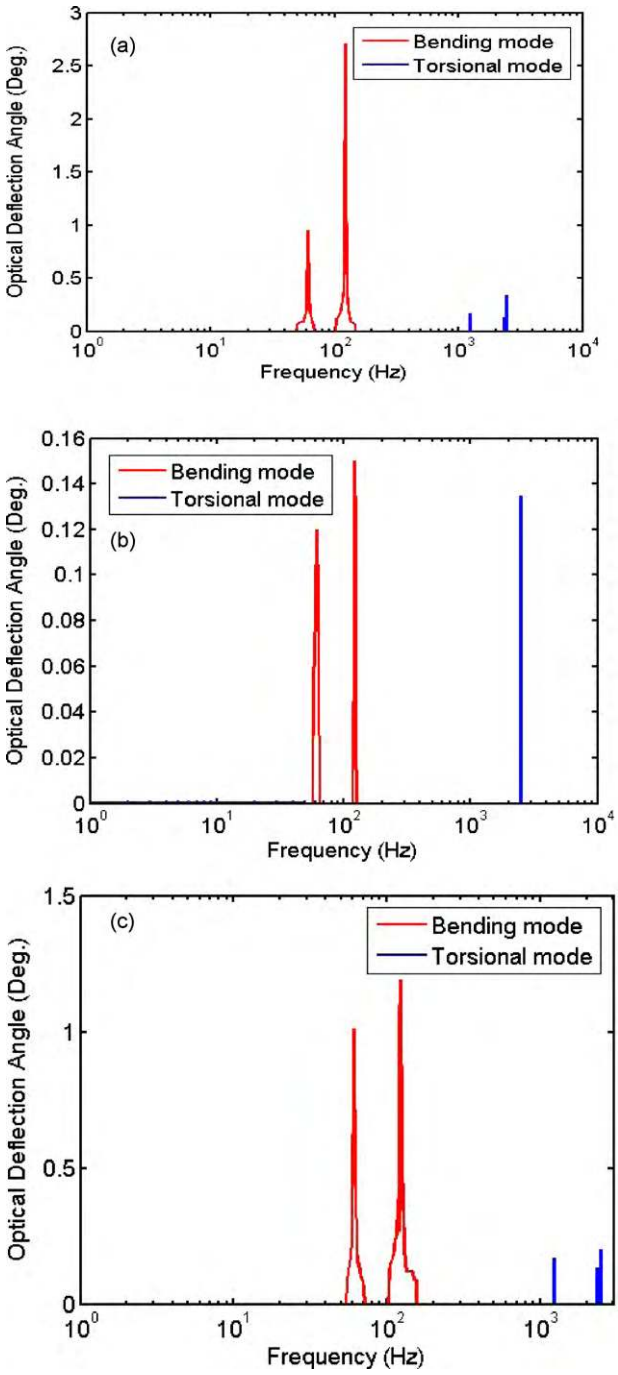

Fig. 14. Spectrum of optical deflection angle versus various ac actuation frequencies observed for both bending and rotation mode for the mirror device B, with (a) the 10th actuator biased at 10 V_{pp} (b) 10 V_{pp} biased serially to actuators 1–6, actuators 7–10 unbiased (c) 10 V_{pp} biased serially to actuators 5–10, actuators 1–4 unbiased.

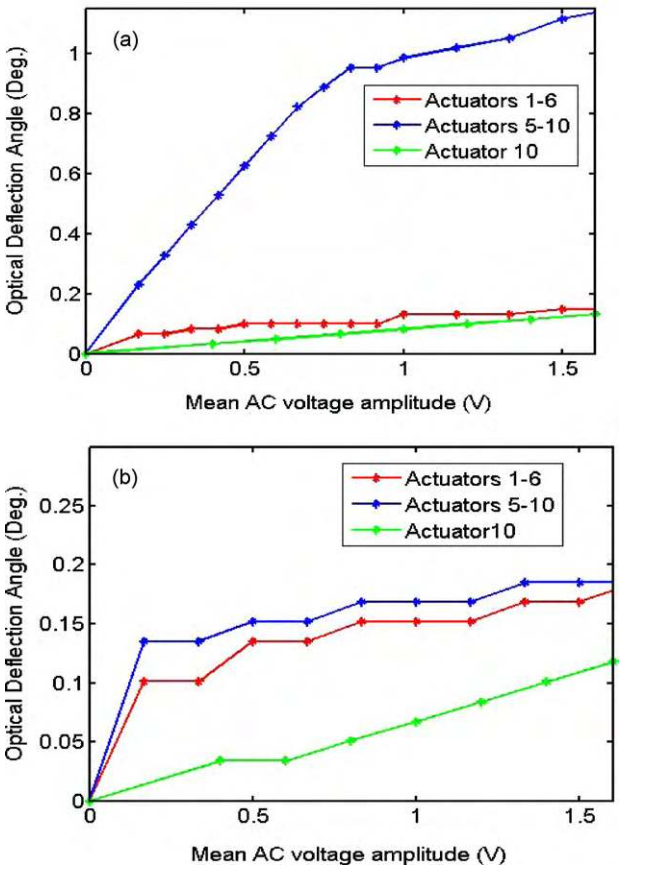

Fig. 15. Measured optical deflection angle of device B versus mean ac driving voltage for different biasing configuration, at (a) bending mode frequency of 122 Hz (b) torsional mode frequency of 2.46 kHz.

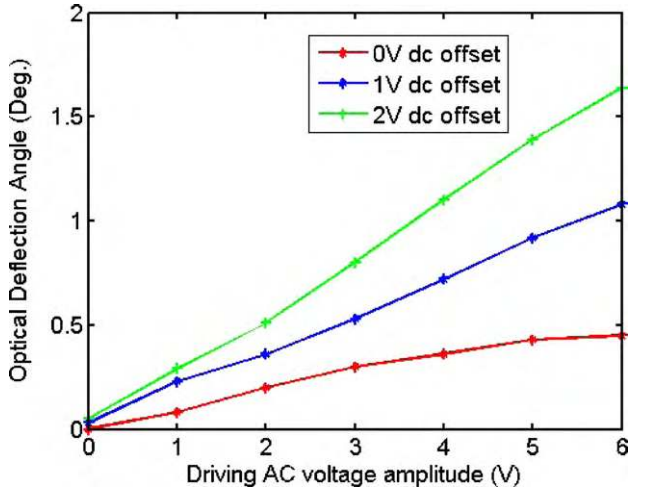

Fig. 16. Measured optical deflection angle of micromirror device B versus ac driving voltage obtained when the 10th actuator is biased simultaneously with an ac voltage at a frequency of 122 Hz and various dc offset.

The ac response of the micromirror device B was studied in Fig. 15. In Fig. 15(a), the piezoelectric characteristic of actuators 1–6 was concluded to be weaker when compared to actuators 5–10 due to the bigger actuation angle by the latter. In addition, the optical deflection angle for micromirror device B is inferior when compared to that of device A. For the same biasing configuration, where actuators 5–10 are serially biased at 9 V_{pp} i.e. mean actuation voltage of each actuator is 1.5 V_{pp}, micromirror device A achieved a slow scanning optical deflection angle of 2.8° whereas device B achieved a much smaller optical deflection angle of 1.15°. For the fast scanning optical deflection angle obtained during torsional mode, micromirror device A again achieved larger angle compared to device B. Despite the differences in optical deflection angle between the two devices, similar trend was noted between them when a dc bias offset was superimposed on ac voltage for both devices. As shown in Fig. 16, for the same ac driving voltage amplitude, a higher dc bias offset results in a better performance. This is due to *in-situ* poling described earlier.

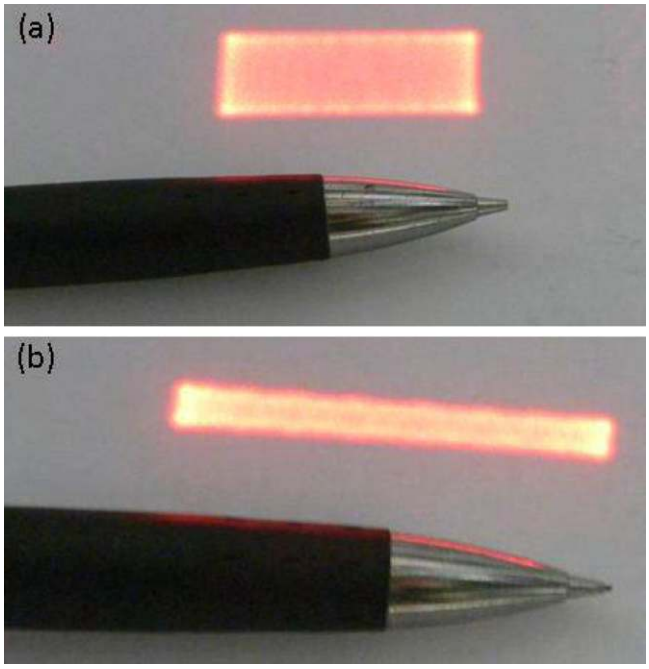

Fig. 17. (a) Lissajous scan pattern obtained when actuators 5–10 are serially biased at 122 Hz, 6 V_{pp}, and actuators 1–4 are serially biased at 2.46 kHz, 10 V_{pp}. (b) Lissajous scan pattern obtained when actuators 1–4 are serially biased at 122 Hz, 10 V_{pp}, while actuators 5–10 are serially biased at 2.46 kHz, 10 V_{pp}.

The laser scanning patterns for micromirror device B are illustrated in Fig. 17. Similar to micromirror device A, to obtain two-dimensional scanning capability, the slow and fast scan drive signals applied to different half of the actuators are superimposed, resulting in Lissajous scan patterns in Fig. 17a and b. In the micromirror device B case, the Lissajous patterns obtained are less distinct due to the smaller slow and fast scan angles.

5.3. Optimized modeling approach

In design of MEMS micromirror, the three main attributes often considered are resolution, dynamic mirror deformation and ratio of slow and fast scan frequency. Besides attributing optical performance to the size of optical deflection angle (2θ), the optical beam divergence caused by unevenness of mirror or deformation during actuation is another factor that has to be taken into consideration. In another words, the optical resolution, defined as the ratio of the optical beam divergence and the mirror scan angle, is a more appropriate performance metric for a scanning mirror. For a perfectly flat mirror under uniform illumination, the far-field intensity distribution is assumed to acquire an Airy pattern. Assuming that the mirror is a circular aperture, the number of resolvable spots, N, can be expressed by [46]:

$$N = 2\frac{d\tan\theta}{1.22\lambda} \tag{10}$$

where d is the diameter of the mirror, α is the mechanical deflection angle (θ), λ is the optical wavelength (632.8 nm).

In addition, dynamic mirror deformation can also contribute to beam divergence, thereby decreasing the optical resolution. The surface deformation δ of a rectangular scanning mirror is given by [47–48]:

$$\delta = 0.183\frac{\rho(1-\nu^2)(2\pi f)^2\theta L^5}{Et^2} \tag{11}$$

where ρ is the material density (Si, 2330 kg m^{-3}), ν is Poisson's ratio of Si (0.27), f is the scan frequency, θ is the mechanical rotation angle, L is the half length of mirror, E is Young's modulus of Si (160 GPa), t is the mirror thickness. From Eq. (11), a thicker Si substrate, smaller mirror size, scanning frequency and rotation angle will result in smaller mirror deformation, hence better quality images. The Rayleigh limit, defined as the maximum amount of surface deformation tolerable without significant degradation in image quality, allows a peak-to-valley surface deformation, δ, of a quarter wavelength, i.e. δ must not exceed 158 nm for a 632.8 nm light source in order to obtain reasonably good resolution images. Hence, in order for micromirror device A to maintain its surface deformation within the Rayleigh limit and achieving a mechanical deflection angle (θ) of 5° at the same time, the resonance frequency of the device is capped at 9.8 kHz. This implies that micromirror device A has excellent dynamic mirror flatness as both the operating frequencies of 34 Hz and 198 Hz required for two-dimensional scanning is well below the maximum frequency allowed. Since both frequencies are far below 9.8 kHz.

The resonant frequency used in torsional mode for fast scanning also affects the optical resolution as it influences the number of columns that can be scanned during the image refresh period. Micromirror device A has a fast vertical scan frequency of 198 Hz, and when combined with 34 Hz slow horizontal scanning signal, results in the definition of 6 columns. To increase the resolution i.e. increase the number of columns defined, the ratio of the fast scan frequency to the slow scan frequency has to be increased.

As such, there are many parameters affecting the resolution of an image, both optically (surface flatness, mirror size, optical deflection angle) and mechanically (ratio of raster scan frequency to frame scan frequency). Improving some of these parameters can increase the image quality directly but depreciate it indirectly at the same time. For example, from Eq. (10), larger mirror size and deflection angle will result in higher resolution. However that is the reverse situation in Eq. (11), where a larger mirror and deflection angle will cause higher surface deformity and hence lower resolution. As a result, an optimum design has to be made, giving priority to some parameters. In our case, optical deflection angle and slow/fast scan frequencies are the two main parameters we hope to improve on.

To enhance our device's mechanical deflection angle, $LaNiO_3$ (LNO) buffered thin film can be deposited during the multilayer deposition of the electrodes [49]. This will improve greatly the transverse piezoelectric constant, d_{31} as the LNO thin films help reduce the degradation caused by wet and dry etching during the microfabrication process.

Fig. 18 shows the simulation done by Abaqus to inspect the effect of mirror dimension and length of PZT cantilever on the resonant frequency for both bending and torsional modes. From Fig. 18(a), for a mirror size of 3 mm × 3 mm, the resonant frequency during bending mode increases from 10 Hz to 36 Hz when the length of PZT cantilever decreases from 7 mm to 3 mm. This makes it equivalent to an increase of 6.5 Hz for every millimeter decrease in cantilever length. However for the same cantilever length, the increase in resonant frequency with decrease in mirror dimension occurs at a much slower rate when compared to the above case. In Fig. 18(b), for a mirror size of 3 mm × 3 mm, the resonant frequency for torsional mode increases from 40 Hz to 220 Hz when the PZT cantilever decreases from 7 mm to 3 mm. This is equivalent to a rate of −45 Hz/mm, which is much higher than the rate of −6.5 Hz/mm in the bending mode case. This implies that for a fixed mirror size, the ratio of fast vertical scan frequency to the slow horizontal scan frequency will increase when the PZT cantilever length decreases. This trend is reflected in Fig. 18(c). In other words, the shorter the PZT cantilever, the higher the resolution of the image. In addition, it can be concluded that changing of mirror dimension might not be worth considering, as it is expected to have limited impact on resolution improvement. This is because from Fig. 18(c), when PZT

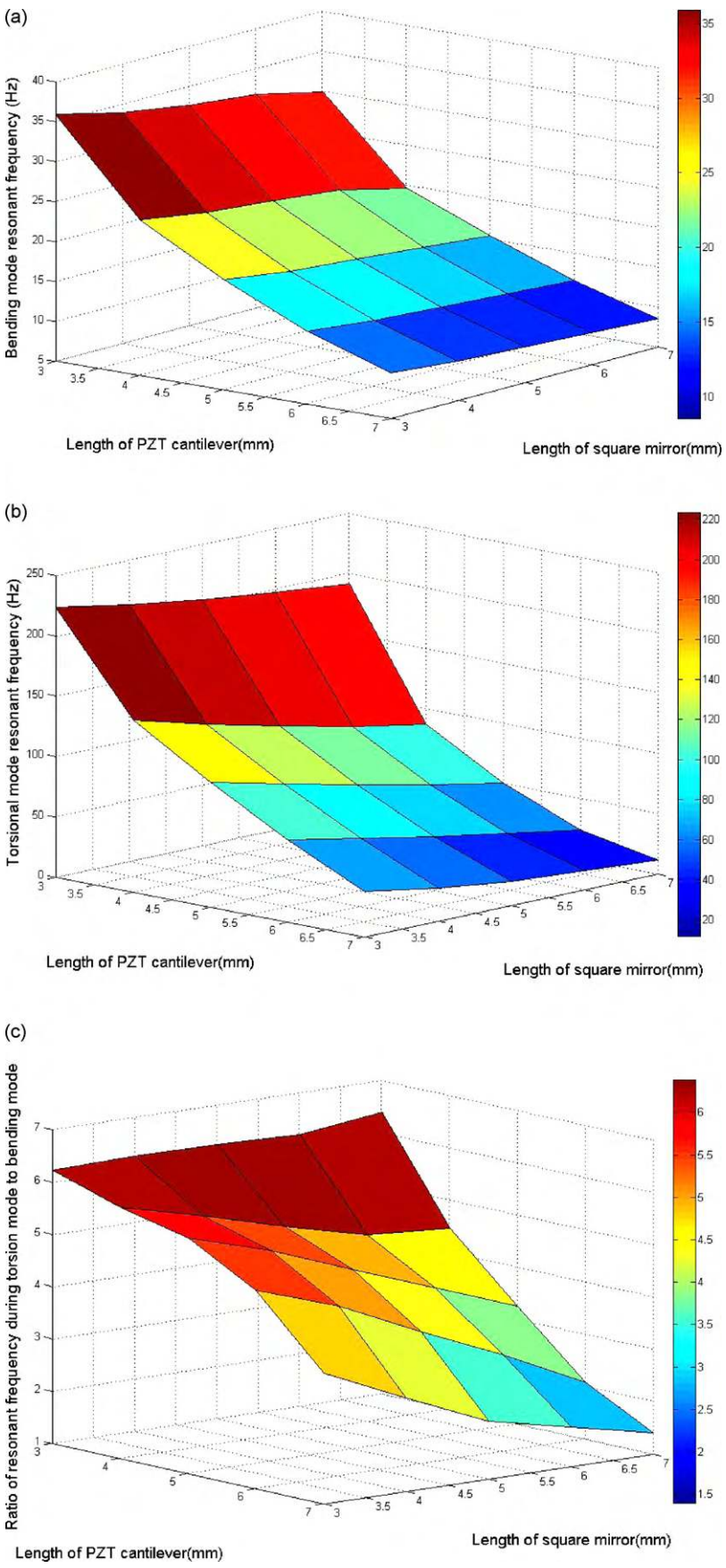

Fig. 18. Topographic diagram by FEA simulation, showing (a) bending mode resonant frequency (b) torsional mode resonant frequency (c) ratio of resonant frequency for torsion mode to bending mode versus various combinations of dimensions for PZT cantilever actuator and mirror.

cantilever length is short, for example 3 mm, the increase in ratio of fast vertical scan frequency to slow horizontal scan frequency for decreasing mirror size occurs at a slower rate when compared to a long PZT cantilever length of, for example, 7 mm. Furthermore, from Eqs. (10) and (11), a change in the mirror dimension will cause an opposing effect on the resolution, hence making the relationship between a mirror's dimension and optical resolution hard to determine. Thus, in order to attain a higher resolution for the current micromirror device at a low mirror surface deformation, a larger value, say 10, for the ratio of the fast vertical scan frequency to slow horizontal scan frequency is strived to be achieved. This may be realized by having a mirror length of 5 mm and cantilever length of 500 μm.

In summary, improvements in optical resolution can be made by increasing the device's mechanical rotation angle and ratio of raster to frame scanning frequency. The former can be implemented by using LNO buffer films during the electrode deposition while the latter can be implemented by decreasing the length of the PZT cantilever actuator. To compensate for the possible increase in dynamic mirror deformation due to larger scanning angle and frequency, a thicker Si substrate can be left beneath the mirror surface to maintain the mirror flatness and rigidity, hence reducing optical beam divergence.

6. Conclusions

Novel piezoelectric driven 2D scanning micromirrors, using a mechanical supporting beam integrated with multiple PZT actuators, have been successfully designed, fabricated and tested. Frequency responses for bending mode operation of both micromirror device A and B were investigated. Micromirror device A and B obtained their slow scanning resonant peak at 34 Hz and 122 Hz respectively, with micromirror device A having an optical angle that can reach as high as 2.8° at 10 V_{pp} applied across 6 series-connected actuators. Torsional mode operation was also examined for both devices. Micromirror device A and B attain their fast scanning resonant peak at 198 Hz and 2.46 kHz respectively, with optical angle reaching up to a maximum of 0.56° at 10 V_{pp} for the bigger device. The effect of superimposed dc bias was also investigated for both devices. With dc bias, a higher optical deflection angle was obtained due to in-situ poling. Symmetric Lissajous scanning patterns for both micromirror device A and B were derived. Finally, optimization approach was discussed such that design trade off analysis was made to meet resolution and frequency requirement of high performance display.

Acknowledgement

The authors would like to acknowledge the support by the National University of Singapore under Grant No. R-263-000-475-112 and the Ph.D scholarship grant received from GLOBALFOUNDRIES Singapore.

References

[1] R.S. Muller, K.Y. Lau, Surface-micromachined microoptical elements and systems, Proc. IEEE 86 (8) (1998) 1705–1720.
[2] J.A. Walker, The future of MEMS in telecommunications networks, J. Micromech. Microeng. 10 (3) (2000) R1–R7.
[3] L.Y. Lin, E.L. Goldstein, Opportunities and challenges for MEMS in lightwave communications, IEEE J. Sel. Top. Quantum Electron. 8 (1) (2002) 163–172.
[4] M. Yano, F. Yamagishi, T. Tsuda, Optical MEMS for photonic switching-compact and stable optical cross connect switches for simple, fast, and flexible wavelength applications in recent photonic networks, IEEE J. Sel. Top. Quantum Electron. 11 (2) (2005) 383–394.
[5] M.C. Wu, O. Solgaard, J.E. Ford, Optical MEMS for lightwave communication, J. Lightwave Technol. 24 (12) (2006) 4433–4454.
[6] C. Lee, J.A. Yeh, Development and evolution of MOEMS technology in variable optical attenuators, J. Micro/Nanolith. MEMS MOEMS 7 (2) (2008) 021003.
[7] C.J. Chang-Hasnain, Tunable VCSEL IEEE J. Sel. Top. Quantum Electron. 6 (6) (2000) 978–987.
[8] A.Q. Liu, X.M. Zhang, A review of MEMS external-cavity tunable lasers, J. Micromech. Microeng. 17 (1) (2007) R1–R13.
[9] J.B. Sampsell, An Overview of Texas Instruments' Digital Micromirror Device (DMD) and its Application to Projection Displays, Society for Information Display International Symposium Digest of Technical Papers, Vol. XXIV, 1012 (1993).
[10] D. Graham-Rowe, Projectors get personal, Nat. Photonics 1 (12) (2007) 667–679.
[11] C.-D. Liao, J.-C. Tsai, The evolution of MEMS display, IEEE Trans. Ind. Electron. 56 (4) (2009) 1057–1065.
[12] W.O. Davis, R. Sprague, J. Miller, MEMS-based pico projector display, in: Opt. MEMS Nanophotonics 2008 IEEE/LEOS Int. Conf., 2008, pp. 31–32.
[13] R. Sanders, D. van Lierop, B. de Jong, H. Soemers, Design and fabrication of a MEMS mirror for miniature laser projection, Proc. SPIE, MOEMS Miniaturized Systems VIII 7208 (2009) 72080R.
[14] A.D. Yalcinkaya, H. Urey, D. Brown, T. Montague, R. Sprague, Two-axis electromagnetic microscanner for high resolution displays, J. Microelectromech. Syst. 15 (4) (2006) 786–794.
[15] H. Miyajima, N. Asaoka, T. Isokawa, M. Ogata, Y. Aoki, M. Imai, O. Fujimori, M. Katashiro, K. Matsumoto, A MEMS electromagnetic optical scanner for a commercial confocal laser scanning microscope, J. Microelectromech. Syst. 12 (3) (2003) 243–251.
[16] H.J. Cho, C.H. Ahn, Magnetically-driven bi-directional optical microscanner, J. Micromech. Microeng. 13 (3) (2003) 383–389.
[17] C.-H. Ji, M. Choi, S.-C. Kim, K.-C. Song, J.-U. Bu, H.-J. Nam, Electromagnetic two-dimensional scanner using radial magnetic field, J. Microelectromech. Syst. 16 (4) (2007) 989–996.
[18] Y.D. Gokdel, B. Sarioglu, S. Mutlu, A.D. Yalcinkaya, Design and fabrication of two-axis ,micromachined steel scanners, J. Micromech. Microeng. 19 (7) (2009).
[19] H. Xie, Y. Pan, G.K. Fedder, A CMOS-MEMS mirror with curled-hinge comb-drives, J. Microelectromech. Syst. 12 (4) (2005) 450–457.
[20] W. Piyawattanametha, P.R. Patterson, D. Hah, H. Toshiyoshi, M.C. Wu, Surface and bulk micromachined two-dimensional scanner driven by angular vertical comb actuators, J. Microelectromech. Syst. 14 (6) (2005) 1329–1338.
[21] J.-C. Tsai, T.-L. Hsieh, C.D. Liao, S.-J. Chiou, D. Hah, M.C. Wu, Experimental characterization of two-axis MEMS scanners with hidden radial vertical comb-drive actuators and cross-bar spring structures, J. Micromech. Microeng. 19 (4) (2009).
[22] C. Lee, Design and fabrication of epitaxial silicon micromirror devices, Sens. Actuators A 115 (2004), pp. 581-500.
[23] D. Lee, U. Krishnamoorthy, K. Yu, O. Solgaard, Single-crystalline silicon micromirrors actuated by self-aligned vertical electrostatic combdrives with piston-motion and rotation capability, Sens. Actuators A 114 (2004) 423–428.
[24] J. Singh, T. Gan, A. Agarwal, Mohanraj, S. Liw, 3D free space thermally actuated micrormirror device, Sens. Actuators A 123–124 (2005) 468–475.
[25] A. Jain, H. Xie, A single crystal silicon micromirror for large bi-directional 2D scanning applications, Sens. Actuators A 130–131 (2006) 454–460.
[26] S.T. Todd, A. Jain, H. Qu, H. Xie, A multi-degree-of-freedom micromirror utilizing inverted-series-connected bimorph actuators, J. Opt. A: Pure Appl. Opt. 8 (7) (2006) 352–359.
[27] L. Wu, H. Xie, Electrothermal micromirror with dual-reflective surfaces for circumferential scanning endoscopic imaging, J. Micro/Nanolith. MEMS MOEMS 8 (1) (2009) 013030.
[28] L. Li, M. Begbie, G. Brown, D. Uttamchandani, Design, simulation and characterization of MEMS optical scanner, J. Micromech. Microeng. 17 (9) (2007) 1781–1787.
[29] A. Schroth, C. Lee, S. Matsumoto, R. Maeda, Application of sol-gel deposited thin PZT film for actuation of 1D and 2D scanners, Sens. Actuators A 73 (1999) 144–152.
[30] F. Filhol, E. Defay, C. Divoux, C. Zinck, M.-T. Delaye, Resonant micro-mirror excited by a thin film piezoelectric actuator for fast optical beam scanning, Sens. Actuators A 123–124 (2005) 483–489.
[31] M. Tani, M. Akamatsu, Y. Yasuda, H. Toshiyoshi, A two-axis piezoelectric tilting micromirror with a newly developed PZT-meandering actuator, IEEE MEMS Int. Conf. 699–702 (2007).
[32] Y. Yasuda, M. Akamatsu, M. Tani, T. Iijima, H. Toshiyoshi, Piezoelectric 2D-optical micro scanners with PZT thick films, Integr. Ferroelectr. 76 (2005) 81–91.
[33] J.-H. Park, J. Akedo, H. Sato, High-speed metal-based optical microscanner using stainless-steel substrate and piezoelectric thick films prepared by aerosol deposition method, Sens. Actuators A 135 (2007) 86–91.
[34] R.A. Conant, J.T. Nee, K.Y. Lau, R.S. Muller, Cyclic fatigue testing of surface-micromachined thermal actuators, ASME Int. Mech. Eng. Congress Exposition 66 (1998) 273–277.
[35] R. Maeda, J.J. Tsaur, S.H. Lee, M. Ichiki, Piezoelectric microactuator devices, J. Electroceram. 12 (2004) 89–100.
[36] S. Trolier-Mckinstry, P. Muralt, Thin film piezoelectrics for MEMS, J. Electroceram. 12 (2004) 7–17.
[37] J.-C. Chiou, C.-F. Kou, Y.-J. Lin, A micromirror with large static rotation and vertical actuation, IEEE J. Sel. Top. Quantum Electron. 13 (2) (2007) 297–303.
[38] S. Schweizer, P. Cousseau, G. Lammel, S. Calmes, Ph. Renaud, Two-dimensional thermally actuated optical microprojector, Sens. Actuators A 85 (2000) 424–429.

[39] S.O. Isikman, O. Ergeneman, A.D. Yalcinkaya, H. Urey, Modeling and characterization of soft magnetic film actuated 2D scanners, IEEE J. Sel. Top. Quantum Electron. 12 (2) (2007) 283–289.
[40] J.G. Smits, W.-S. Choi, The constituent equations of piezoelectric heterogeneous bimorphs, IEEE Trans. Ultrason., Ferroelectr. Frequency Control 38 (3) (1991) 256–270.
[41] T. Kobayashi, M. Ichiki, J. Tsaur, R. Maeda, Effect of multi-coating process on the orientation and microstructure of lead zirconate titanate (PZT) thin films derived by chemical solution deposition, Thin Solid Films 489 (2005) 74–78.
[42] T. Kobayashi, M. Ichiki, R. Kondou, K. Nakamura, R. Maeda, Fabrication of piezoelectric microcantilevers using $LaNiO_3$ buffered $Pb(Zr,Ti)O_3$ thin film, J. Micromech. Microeng. 18 (2008).
[43] T. Kobayashi, R. Maeda, T. Itoh, Low speed piezoelectric optical microscanner actuated by piezoelectric microcantilevers using $LaNiO_3$ buffered $Pb(Zr,Ti)O_3$ thin film, Smart Mater. Struct. 18 (2009) 065008-1–165008-6.
[44] T. Kobayashi, M. Ichiki, T. Noguchi, K. Nakamura, R. Maeda, Deflectioni of wafers and cantilevers with Pt/LNO/PZT/LNO/Pt/Ti/SiO2 multilayered structures, Thin Solid Films 516 (2008) 035007-1–135007-5.
[45] T. Kobayashi, R. Maeda, T. Itoh, The influence of dc bias on the displacement and sensor output of sensitive piezoelectric microcantilevers, J. Micromech. Microeng. 18 (3) (2008).
[46] E. Hecht, Optics, 3rd ed., Pergamon, 1998.
[47] P.J. Brosen, Dynamic mirror distortion in optical scanning, Appl. Opt. 11 (12) (1972) 2987–2989.
[48] R.A. Conant, J.T. Nee, K.Y. La", R.S. Muller, A flat high frequency scanning micromirror, Solid State Sensor Actuator Workshop (2000) 6–9.
[49] T. Kobayashi, M. Ichiki, R. Kondou, K. Nakamura, R. Maeda, Fabrication of piezoelectric microcantilevers using $LaNiO_3$ buffered $Pb(Zr,Ti)O_3$ thin film, J. Micromech. Microeng. 18 (3) (2008).

Biographies

Kah How Koh received his B.Eng. degree in Electrical Engineering from Department of Electrical and Computer Engineering in 2009. He is currently a Ph. D. student in the same department at National University of Singapore, Singapore, in 2009. His research interests include optical MEMS, focusing on scanning mirror and variable optical attenuator.

Takeshi Kobayashi received his B.S. and M.S. degree in Materials Science from The University of Tokyo. He also received Ph. D degree in Materials Science from The University of Tokyo in 2002. He worked as researcher in National Institute of Advance Industrial Science and Technology (AIST), Japan. His research interest includes piezoelectric MEMS devices and their application to wireless sensor network. He has contributed to 30 international journal papers and 21 conference proceedings. Two of his recent publications have been selected as highlighted paper of Journal of Micromechanics and Microengineering in 2007 and 2008.

Fu-Li Hsiao received his B.S. degree in the Department of Physics of National Changhua University of Education, Taiwan, in 2002 and the Ph. D. degree in Department of Optics and Photonics of National Central University, Taiwan, and FEMTO-ST of University of Franche-Comte, France, in 2008. He was a Research Fellow in the Department of Electrical and Computer Engineering of National University of Singapore. He is currently an Assistant Professor for Graduate Institute of Photonics in National Changhua University of Education, Taiwan. His research interests include photonic crystals, optical MEMS and phononic crystals.

Chengkuo Lee received his M.S. degree in Materials Science and Engineering from National Tsing Hua University, Hsinchu, Taiwan, in 1991. He also received a M.S. degree in Industrial and System Engineering from Rutgers University, New Brunswick, NJ, USA in 1993. He received the Ph.D. degree in Precision Engineering from the University of Tokyo, Tokyo, Japan, in January 1996. He worked as foreign researcher in the Nanometer-scale Manufacturing Science Lab. at Research Center for Advanced Science and Technology (RCAST) of the University of Tokyo from 1993 to 1996. He had also worked in Mechanical Engineering Lab., AIST, MITI of Japan as a JST research fellow in 1996. Thereafter he was a senior research staff of Microsystems Lab., Industrial Technology Research Institute (ITRI), Hsinchu, Taiwan. Since September 1997, he has joined the Metrodyne Microsystem Corporation, Hsinchu, Taiwan, and established the MEMS device division and the 1st micromachining fab for commercial purpose in Taiwan. He was the manager of MEMS device division between 1997 and 2000. He had been the adjunct assistant professor in Electrophysics Department of National Chiao Tung University in 1998, and the adjunct assistant professor in Institute of Precision Eng. of National Chung Hsing University since 2001 to 2005. He co-founded the Asia Pacific Microsystems, Inc. (APM) Hsinchu, Taiwan, in August 2001, and he has been the vice president (VP) of R&D at the beginning, then become the VP of optical communication business unit and special assistant of CEO in charge of international business and technical marketing for MEMS foundry service at APM, Inc. till end of 2005. APM has achieved annual revenue of 13M US$ in 2005 and was ranked as top number 30 of world MEMS manufacturers in 2004. Currently He is an assistant professor at the Dept. of Electrical and Computer Eng. of National University of Singapore and a senior member of technical staff at the Institute of Microelectronics (IME), A*Star, Singapore. He has contributed more than 130 international conference papers and extended abstracts, 75 peer-reviewed international journal articles, and 9 US patents in MEMS and Nanotechnology field. He is the member of IEEE, MRS, and IEE Japan.